



HAL
open science

Spectroscopy of solid-solution transparent sesquioxide laser ceramic Tm:LuYO₃

Kirill Ereemeev, Pavel Loiko, Alain Braud, Patrice Camy, Jian Zhang, Xiaodong Xu, Yongguang Zhao, Peng Liu, Stanislav Balabanov, Elena Dunina, et al.

► **To cite this version:**

Kirill Ereemeev, Pavel Loiko, Alain Braud, Patrice Camy, Jian Zhang, et al.. Spectroscopy of solid-solution transparent sesquioxide laser ceramic Tm:LuYO₃. *Optical Materials Express*, 2022, 12 (9), pp.3749. 10.1364/OME.471492. hal-04211112

HAL Id: hal-04211112

<https://hal.science/hal-04211112>

Submitted on 1 Nov 2023

HAL is a multi-disciplinary open access archive for the deposit and dissemination of scientific research documents, whether they are published or not. The documents may come from teaching and research institutions in France or abroad, or from public or private research centers.

L'archive ouverte pluridisciplinaire **HAL**, est destinée au dépôt et à la diffusion de documents scientifiques de niveau recherche, publiés ou non, émanant des établissements d'enseignement et de recherche français ou étrangers, des laboratoires publics ou privés.

Spectroscopy of solid-solution transparent sesquioxide laser ceramic Tm:LuYO₃

KIRILL EREMEEV,¹ PAVEL LOIKO,¹ ALAIN BRAUD,¹ PATRICE CAMY,¹ JIAN ZHANG,² XIAODONG XU,³ YONGGUANG ZHAO,³ PENG LIU,³ STANISLAV BALABANOV,⁴ ELENA DUNINA,⁵ ALEXEY KORNIENKO,⁵ LIUDMILA FOMICHEVA,⁶ XAVIER MATEOS,⁷ UWE GRIEBNER,⁸ VALENTIN PETROV,⁸ LI WANG,⁸ AND WEIDONG CHEN^{8,9,*}

¹Centre de Recherche sur les Ions, les Matériaux et la Photonique (CIMAP), UMR 6252 CEA-CNRS-ENSICAEN, Université de Caen, 6 Boulevard du Maréchal Juin, 14050 Caen Cedex 4, France

²Key Laboratory of Transparent and Opto-Functional Inorganic Materials, Shanghai Institute of Ceramics, Chinese Academy of Sciences, 201800 Shanghai, China

³Jiangsu Key Laboratory of Advanced Laser Materials and Devices, Jiangsu Normal University, 221116 Xuzhou, China

⁴G. G. Devyatikh Institute of Chemistry of High-Purity Substances of the Russian Academy of Sciences, 603951 Nizhny Novgorod, Russia

⁵Vitebsk State Technological University, 72 Moskovskaya Ave., 210035 Vitebsk, Belarus

⁶Belarusian State University of Informatics and Radioelectronics, 6 Brovka St., 220027, Minsk, Belarus

⁷Universitat Rovira i Virgili, URV, Física i Cristal·lografia de Materials, (FiCMA)- Marcel·li Domingo 1, 43007 Tarragona, Spain

⁸Max Born Institute for Nonlinear Optics and Short Pulse Spectroscopy, Max-Born-Str. 2a, D-12489 Berlin, Germany

⁹Fujian Institute of Research on the Structure of Matter, Chinese Academy of Sciences, 350002 Fuzhou, China

*chenweidong@fjirsm.ac.cn

Abstract: We report on a detailed spectroscopic study of a Tm³⁺-doped transparent sesquioxide ceramic based on a solid-solution (lutetia – yttria, LuYO₃) composition. The ceramic was fabricated using commercial oxide powders by hot isostatic pressing at 1600°C for 3 h at 190 MPa argon pressure. The most intense Raman peak in Tm:LuYO₃ at 385.4 cm⁻¹ takes an intermediate position between those for the parent compounds and is notably broadened (linewidth: 12.8 cm⁻¹). The transition intensities of Tm³⁺ ions were calculated using the Judd-Ofelt theory; the intensity parameters are $\Omega_2 = 2.537$, $\Omega_4 = 1.156$ and $\Omega_6 = 0.939$ [10²⁰ cm²]. For the ³F₄ → ³H₆ transition, the stimulated-emission cross-section amounts to 0.27×10⁻²⁰ cm² at 2059 nm and the reabsorption-free luminescence lifetime is 3.47 ms (the ³F₄ radiative lifetime is 3.85±0.1 ms). The Tm³⁺ ions in the ceramic exhibit long-wave multiphonon-assisted emission extending up to at least 2.35 μm; a phonon sideband at 2.23 μm is observed and explained by coupling between electronic transitions and the dominant Raman mode of the sesquioxides. Low temperature (12 K) spectroscopy reveals a significant inhomogeneous spectral broadening confirming formation of a substitutional solid-solution. The mixed ceramic is promising for ultrashort pulse generation at >2 μm.

© 2022 Optica Publishing Group under the terms of the [Optica Publishing Group Open Access Publishing Agreement](#)

1. Introduction

Rare-earth sesquioxides R₂O₃ (where R is a lanthanide, Y or Sc) represent an important class of optical materials. The most interesting form of R₂O₃ compounds is the cubic one (also called C-type, sp. gr. Ia $\bar{3}$, bixbyite structure). Cubic rare-earth sesquioxides such as Y₂O₃ (yttria), Sc₂O₃ (scandia) or Lu₂O₃ (lutetia) are known as excellent host media for doping with trivalent rare-earth ions (RE³⁺) [1]. As host matrices, they feature good thermo-mechanical

48 and thermo-optical properties [2,3] (i.e., high thermal conductivity with weak dependence on
49 the doping level, weak isotropic thermal expansion, small and positive dn/dT coefficient), low
50 phonon energies (for oxide materials), and wide transparency [4]. The RE^{3+} dopant ions
51 substitute for the host-forming R^{3+} metal cations in two types of sites (C_2 and C_{3i} symmetry)
52 with VI-fold oxygen coordination [5,6]. However, the spectroscopic properties of RE^{3+} -doped
53 R_2O_3 compounds are mainly determined by C_2 species (about 3/4 of ions) since for the
54 centrosymmetric C_{3i} ones (about 1/4 of ions), the electric dipole transitions are not enabled
55 [1]. The RE^{3+} ions in cubic sesquioxides experience strong crystal fields leading to large Stark
56 splitting of their multiplets and, consequently, broad emission bands. The crystal-field
57 strength increases in the series $R^{3+} = Y^{3+} \rightarrow Lu^{3+} \rightarrow Sc^{3+}$ according to the variation of the
58 ionic radius, making it possible to alter the spectral properties by changing the host
59 composition [7].

60 The main drawback of R_2O_3 crystals are their extremely high melting points (e.g. 2425°C
61 for Y_2O_3) complicating the crystal growth. So far different techniques have been used for
62 growing R_2O_3 crystals, such as heat exchanger growth method (HEM), micro-pulling-down
63 (μ -PD), Czochralski (Cz), etc. [8,9]. Still, single-crystals suffer from coloration, Rhenium
64 (Re) impurities (when using Re crucibles), and a gradient of RE^{3+} dopant concentration
65 (especially for Sc_2O_3). During the past decades, the transparent ceramic technology emerged
66 as a competitive approach to the single-crystal growth [10]. It offers: (i) much lower synthesis
67 temperatures (<1800°C); (ii) easier RE^{3+} doping in terms of higher available concentrations
68 and more uniform ion distribution; (iii) well-preserved spectroscopic and thermal properties;
69 (iv) possibility to fabricate mixed compositions $(R_1,R_2)_2O_3$ with well-controlled R_1/R_2 ratio;
70 and (v) size-scalability. Laser-quality RE^{3+} -doped yttria [11,12], lutetia [13,14] and scandia
71 [15] ceramics have been developed. The main challenge for ceramics is reaching high
72 transparency close to the theoretical limit (i.e., weak light scattering owing to residual pores,
73 possible secondary phases at the grain boundaries, etc.).

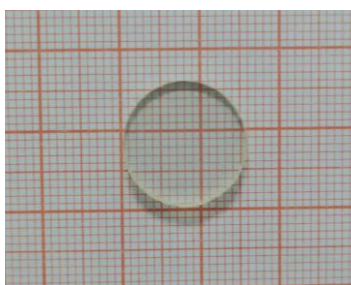
74 Substitutional solid solutions $A_{1-x}B_x$ ($0 < x < 1$) also called “mixed” materials are
75 attracting attention for tailoring the spectroscopic properties of the dopant RE^{3+} ions [16-19]
76 as, under the condition of different crystal-field strengths associated with the parent
77 compounds A and B, the absorption / emission lines of the dopants may experience strong
78 inhomogeneous broadening. For cubic sesquioxides, isostructural solid-solutions with a
79 general composition $(Y_{1-x-y}Lu_xSc_y)_2O_3$ exist in the full range of x and y . The same is true also
80 for mixing with some active RE^{3+} ions, as long as their stoichiometric compositions (RE_2O_3)
81 possess the same cubic symmetry, e.g. Yb, Tm, Ho or Er. Although the growth of “mixed”
82 sesquioxide crystals has been reported [19,20], it is much easier to fabricate such compounds
83 via a transparent ceramic technology. Recently, laser ceramics in the lutetia-scandia and
84 lutetia-yttria binary systems were developed [16,18,21-25].

85 Thulium (Tm^{3+}) doped sesquioxides attract attention because of their suitability for
86 efficient lasing around 2 μm according to the $^3F_4 \rightarrow ^3H_6$ electronic transition [26]. Tm^{3+} ions
87 experience strong crystal-fields in R_2O_3 compounds. The resulting substantial Stark splitting
88 of their multiplets determines broad emission spectra naturally extending above 2 μm [7]. The
89 latter property is of practical importance for broadly tunable and especially mode-locked
90 lasers [27,28] as this helps to avoid the structured water vapor absorption in the atmosphere
91 spectrally located at < 2 μm which is detrimental for achieving femtosecond pulses. Recently,
92 femtosecond mode-locked Tm ceramic lasers based on “mixed” sesquioxides such as
93 $Tm:(Lu,Sc)_2O_3$ and $Tm:(Lu,Y)_2O_3$ were reported [28-30].

94 The present work is devoted to the spectroscopic properties of Tm^{3+} ions in a “mixed”
95 (lutetia – yttria) sesquioxide laser ceramic, with the goal of revealing the effect of
96 compositional disorder on the inhomogeneous broadening of absorption and emission lines, in
97 order to better understand the potential of such materials for generation of few-optical-cycle
98 pulses.

99 2. Synthesis of transparent ceramics

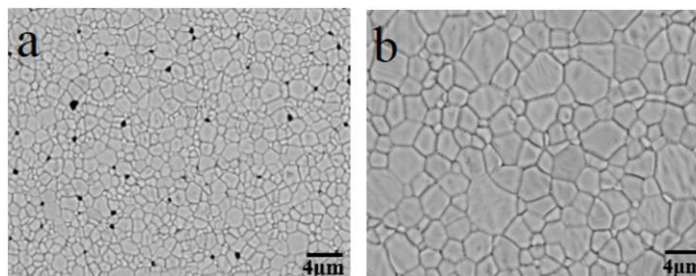
100 Commercial powders of rare-earth oxides, Lu_2O_3 (purity: 4N), Y_2O_3 (5N) and Tm_2O_3 (4N),
101 from Jiahua Advanced Material Resources, China, were used as raw materials. They were
102 weighed according to the composition of 3.0 at.% $\text{Tm}:(\text{Lu}_{0.5}\text{Y}_{0.5})_2\text{O}_3$. The mixed powders
103 were ball-milled in ethanol for 24 h with 1.0 at.% monoclinic ZrO_2 powder (Shandong
104 Sinocera Functional Material, China) serving as a sintering aid. The milled slurries were dried
105 in an oven at 70°C for 24 h and then sieved through a 100-mesh screen. After that, the
106 powders were dry-pressed into pellets by a 12 mm-diameter mold and cold isostatically
107 pressed at 200 MPa for 5 min. All the green bodies were calcined at 850°C for 4 h to remove
108 the residue organics. After that, the samples were first pre-sintered at 1650°C for 4 h in
109 vacuum under a pressure lower than 1.0×10^{-3} Pa, equipped with a tungsten mesh as the
110 heating element. Then, the pre-sintered ceramics were treated by hot isostatic pressing
111 (HIPing) at 1600°C for 3 h in 190 MPa argon pressure to eliminate residual pores. Finally, the
112 HIP-treated samples were annealed at 1200°C for 24 h in a muffle furnace in air to
113 compensate the oxygen loss during the vacuum pre-sintering and the following HIP
114 treatment. Then, the ceramic disks were polished on both sides to laser quality level, Fig. 1.
115 The obtained ceramic disks were transparent and slightly yellow colored due to the Tm^{3+}
116 doping. The calculated Tm^{3+} ion density in the “mixed” ceramic was $N_{\text{Tm}} = 8.34 \times 10^{20}$ at/ cm^3 .



117
118

Fig. 1. A photograph of annealed and polished 3.0 at.% $\text{Tm}:\text{LuYO}_3$ ceramic disk.

119 To observe the microstructure of the ceramic, its polished surface was thermally etched at
120 1400°C for 2 h in a muffle furnace in air. The thermally etched surfaces of the 3.0 at.%
121 $\text{Tm}:\text{LuYO}_3$ ceramics before and after HIPing were characterized using a Scanning Electron
122 Microscope (SEM, TM3000, Hitachi, Japan). The pre-sintered ceramic has an average grain
123 size of $1 \mu\text{m}$ and it contains sub- μm sized pores localized at the grain boundaries, Fig. 2(a).
124 After HIPing, the mean grain size increases to $2.4 \mu\text{m}$. The ceramic exhibits a close-packed
125 microstructure with clean grain boundaries, Fig. 2(b).



126
127
128

Fig. 2. SEM images of the thermally etched surface of the 3.0 at.% $\text{Tm}:\text{LuYO}_3$ ceramics: (a) a pre-sintered sample; (b) a sample after HIPing.

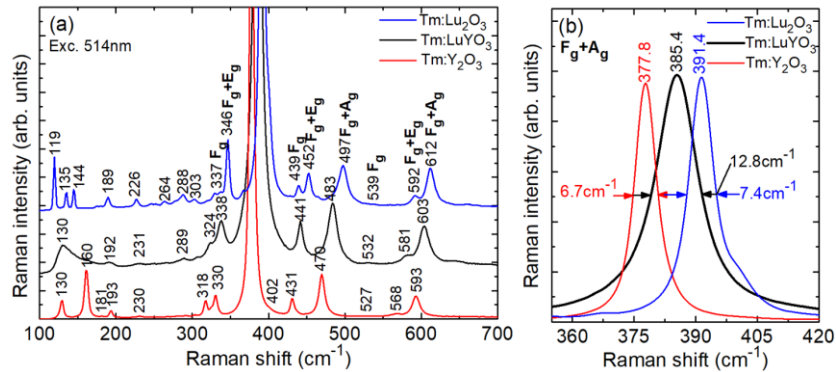
129 For comparison, two parent ceramics, $\text{Tm}:\text{Lu}_2\text{O}_3$ and $\text{Tm}:\text{Y}_2\text{O}_3$, doped with 3 at.% Tm^{3+}
130 ($N_{\text{Tm}} = 8.61 \times 10^{20} \text{ cm}^{-3}$ and $7.85 \times 10^{20} \text{ cm}^{-3}$, respectively), were fabricated.

131 3. Results and discussion

132 **3.1 Raman spectra**

133 The room temperature (RT) Raman spectra were measured using a confocal laser microscope
 134 (Renishaw inVia) equipped with a $\times 50$ Leica objective and an Ar⁺ ion laser (514 nm). For
 135 cubic sesquioxides (sp. gr. $Ia\bar{3}$) possessing a body-centered structure, the factor group
 136 analysis predicts the following irreducible representations for the optical and acoustical
 137 modes at the center of the Brillouin zone ($\mathbf{k} = 0$): $\Gamma_{op} = 4A_g + 4E_g + 14F_g + 5A_{2u} + 5E_u + 16F_u$
 138 (of which 22 modes (A_g , E_g , and F_g) are Raman-active, 16 modes (F_u) are IR-active, and the
 139 rest are silent) and $\Gamma_{ac} = F_u$ [31,32].

140 Figure 3(a) shows the Raman spectra of the Tm³⁺-doped LuYO₃, Y₂O₃ and Lu₂O₃
 141 ceramics. They are typical for cubic (C-type) sesquioxides. The vibrational spectra exhibit
 142 two distinct frequency ranges: the relative position and intensities of the modes above
 143 300 cm⁻¹ are rather similar for different ceramic compositions indicating that they are most
 144 probably related to oxygen motions and deformations of the [AO₆] octahedrons [31]. The
 145 most intense peak is assigned to $F_g + A_g$ vibrations [31], Fig. 3(b). For the yttria and lutetia
 146 ceramics, it is centered at 377.8 and 391.4 cm⁻¹, respectively, and its linewidth is nearly the
 147 same (6.7 and 7.4 cm⁻¹, respectively). For the “mixed” ceramic, this peak takes an
 148 intermediate position (385.4 cm⁻¹) and it is notably broadened (linewidth: 12.8 cm⁻¹)
 149 confirming the formation of a substitutional solid-solution. A similar tendency is observed for
 150 other well assigned modes in the high-frequency range of $\sim 300 - 600$ cm⁻¹. The peak
 151 corresponding to the maximum phonon energy (the $F_g + A_g$ vibrations) is observed at 593 cm⁻¹
 152 (Tm:Y₂O₃), 603 cm⁻¹ (Tm:LuYO₃) and 612 cm⁻¹ (Tm:Lu₂O₃).



153 **Fig. 3.** Unpolarized Raman spectra of Tm³⁺-doped Lu₂O₃, Y₂O₃ and LuYO₃ ceramics: (a)
 154 overview spectra; (b) a close look at the most intense mode ($F_g + A_g$), $\lambda_{exc} = 514$ nm. Numbers
 155 indicate the Raman frequencies in cm⁻¹.
 156

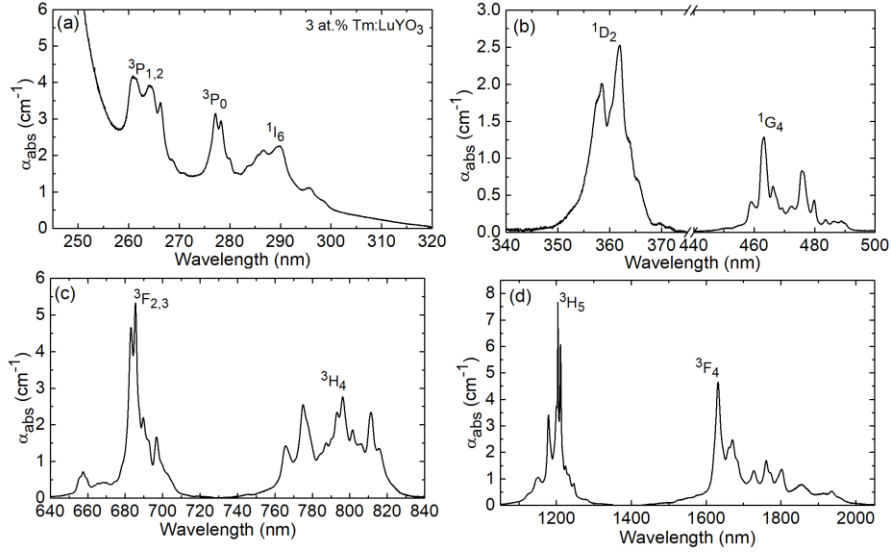
157 **3.2 Absorption spectra and Judd-Ofelt analysis**

158 The transmission / absorption spectra were measured using a spectrophotometer (Lambda
 159 1050, Perkin Elmer).

160 The Tm:LuYO₃ ceramic exhibited a relatively high linear transmission of 81.5% at 2.2 μ m
 161 (out of the Tm³⁺ absorption bands), close to the theoretical limit, $T_0 = 2n/(n^2 + 1) = 82.0\%$ (a
 162 formula accounting for multiple light reflections, $n = 1.918$ is the estimated refractive index
 163 of LuYO₃ [33]). The absorption spectrum of Tm³⁺ ions in the “mixed” ceramic is shown in
 164 Fig. 4. Bands related to transitions from the ground-state (³H₆) to the excited-states ranging
 165 from ³F₄ up to ³P_{0,2} are observed. The UV absorption edge is observed at ~ 250 nm (for
 166 undoped Lu₂O₃, the optical bandgap E_g is 5.6 eV [34] or ~ 221 nm).

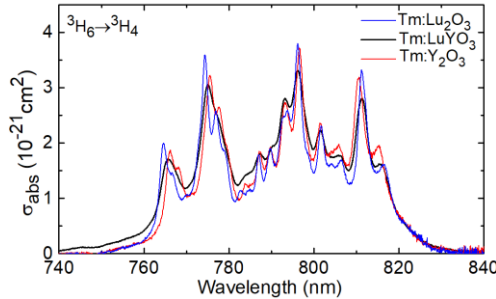
167 The absorption cross-sections σ_{abs} for the ³H₆ \rightarrow ³H₄ transition of Tm³⁺ in the “mixed”
 168 LuYO₃ ceramic, and in Y₂O₃ and Lu₂O₃, are shown in Fig. 5. This absorption band is suitable
 169 for pumping Tm-lasers using commercially available AlGaAs diode lasers emitting around
 170 0.8 μ m. For the “mixed” ceramic, the absorption spectrum is broadened as compared to both

171 parent compounds; the maximum σ_{abs} is $0.33 \times 10^{-20} \text{ cm}^2$ at 796.2 nm corresponding to an
 172 absorption bandwidth $\Delta\lambda_{\text{abs}}$ of $\sim 21 \text{ nm}$ (combining several peaks), compared with
 173 $\sigma_{\text{abs}} = 0.37 \times 10^{-20} \text{ cm}^2$ at 796.7 nm with $\Delta\lambda_{\text{abs}}$ of $\sim 7 \text{ nm}$ for the Tm:Y₂O₃ ceramic.



174
 175
 176

Fig. 4. RT absorption spectra of the 3 at.% Tm:LuYO₃ ceramic in the spectral range of (a) 245 – 320 nm, (b) 340 – 500 nm, (c) 640 – 840 nm, (d) 1050 – 2050 nm.



177
 178
 179

Fig. 5. Absorption cross-sections, σ_{abs} , for the $^3H_6 \rightarrow ^3H_4$ transition of Tm³⁺ ions in the LuYO₃, Y₂O₃ and Lu₂O₃ ceramics.

180 The measured absorption spectrum was analyzed using the standard Judd-Ofelt (J-O)
 181 theory [35,36]. Eight Tm³⁺ transitions were considered. The set of reduced squared matrix
 182 elements $U^{(k)}$ was taken from [37]. The magnetic-dipole (MD) contributions to transition
 183 intensities (for transitions with $\Delta J = J - J' = 0, \pm 1$) were calculated within the Russel-Saunders
 184 approximations using the wave functions of the free Tm³⁺ ion. The refractive index of the
 185 “mixed” ceramic LuYO₃ was calculated using the dispersion curves of the parent compounds
 186 [34]. More details about the J - O analysis can be found elsewhere [38].

187 For calculating the absorption oscillator strengths, we have used the full Tm³⁺ ions density
 188 (N_{Tm}), although some authors suggest to account only for ions located in C₂ sites [$\sim(3/4)N_{\text{Tm}}$]
 189 [39]. However, for a “mixed” ceramic, the actual distribution of dopant ions over the C₂ and
 190 C_{3i} sites may significantly differ from that for the parent material.

191 Table I contains the experimental (f_{exp}^{Σ}) and calculated (f_{calc}^{Σ}) absorption oscillator
 192 strengths. Here, the superscript “ Σ ” indicates a total value (ED + MD). The root mean square
 193 (r.m.s.) deviation between the f_{exp}^{Σ} and f_{calc}^{Σ} values is $\delta_{\text{rms}} = 1.202$, mainly due to the
 194 transitions to thermally coupled levels $^3F_2 + ^3F_3$ and $^1I_6 + ^3P_0 + ^3P_1$. For the lowest-lying

195 excited-state (3F_4), a relatively good agreement is observed. The corresponding J - O
 196 parameters are $\Omega_2 = 2.537$, $\Omega_4 = 1.156$ and $\Omega_6 = 0.939$ [10^{20} cm 2]. These values agree well
 197 with those reported recently for another Tm $^{3+}$ -doped “mixed” sesquioxide ceramic with a
 198 composition (Lu,Sc) $_2$ O $_3$, $\Omega_2 = 2.429$, $\Omega_4 = 1.078$ and $\Omega_6 = 0.653$ [10^{20} cm 2] [16].

199 **Table 1. Experimental and Calculated Absorption Oscillator Strengths^a for Tm $^{3+}$ Ions in LuYO $_3$**

Transition	$\langle\lambda_{\text{abs}}\rangle$, nm	$\langle E \rangle$, cm $^{-1}$	$\langle n \rangle$	Γ , cm $^{-1}$ nm	$f_{\text{exp}}^{\text{E}} \times 10^6$	$f_{\text{calc}}^{\text{E}} \times 10^6$
$^3H_6 \rightarrow ^3F_4$	1763	5672	1.912	444.25	2.038	2.126 ^{ED}
$^3H_6 \rightarrow ^3H_5$	1206	8292	1.921	243.02	2.308	1.458 ^{ED} +0.530 ^{MD}
$^3H_6 \rightarrow ^3H_4$	795	12585	1.933	101.29	2.192	2.562 ^{ED}
$^3H_6 \rightarrow ^3F_2 + ^3F_3$	684	14616	1.939	68.308	1.977	3.216 ^{ED}
$^3H_6 \rightarrow ^1G_4$	473	21155	1.964	14.359	0.881	0.753 ^{ED}
$^3H_6 \rightarrow ^1D_2$	361	27738	2.009	20.231	2.117	2.114 ^{ED}
$^3H_6 \rightarrow ^1I_6 + ^3P_0 + ^3P_1$	284	35178	2.084	24.788	4.131	1.778 ^{ED} +0.029 ^{MD}
$^3H_6 \rightarrow ^3P_2$	263	37968	2.126	13.235	2.585	2.411 ^{ED}
δ_{rms}						1.202

200 ^a $\langle\lambda_{\text{abs}}\rangle$ - “center of gravity” of the absorption band, $\langle E \rangle$ - energy barycenter of the multiplet, $\langle n \rangle$ - mean
 201 refractive index, Γ - integrated absorption coefficient, $f_{\text{exp}}^{\text{E}}$ and $f_{\text{calc}}^{\text{E}}$ - experimental and calculated
 202 absorption oscillator strengths, respectively, ED and MD - electric and magnetic dipole, respectively.

203 Using the determined J - O parameters, the probabilities (ED + MD) of spontaneous
 204 radiative transitions for particular emission channels $J \rightarrow J' A_{\Sigma}^{\text{calc}}(JJ')$, the total probabilities of
 205 radiative transitions from excited-states $A_{\text{tot}} = \sum_j A_{\Sigma}^{\text{calc}}(JJ')$, the luminescence branching ratios
 206 $B(JJ') = A_{\Sigma}^{\text{calc}}(JJ')/A_{\text{tot}}$ and the radiative lifetimes $\tau_{\text{rad}} = 1/A_{\text{tot}}$ were calculated, cf. Table 2. The
 207 mean emission wavelengths $\langle\lambda_{\text{em}}\rangle$ were estimated using the barycenter energies of Tm $^{3+}$
 208 multiplets $\langle E \rangle$ from Table 1. For the 3F_4 and 3H_4 states, τ_{rad} amounts to 4.18 ms and 0.61 ms,
 209 respectively.

210 **Table 2. Calculated Emission Probabilities^a for Tm $^{3+}$ Ions in LuYO $_3$**

Excited state	Terminal state	$\langle\lambda_{\text{em}}\rangle$, nm	$A_{\Sigma}^{\text{calc}}(JJ')$, s $^{-1}$	$B(JJ')$, %	A_{tot} , s $^{-1}$	τ_{rad} , ms
3F_4	3H_6	1763.0	239.36 ^{ED}	100	239.36	4.178
3H_5	3F_4	3816.8	9.69 ^{ED} + 0.26 ^{MD}	2.5	406.09	2.463
	3H_6	1206.0	291.03 ^{ED} + 105.11 ^{MD}	97.5		
3H_4	3H_5	2329.4	25.20 ^{ED} + 10.48 ^{MD}	2.2	1649.19	0.606
	3F_4	1446.5	122.23 ^{ED} + 27.27 ^{MD}	9.1		
	3H_6	794.6	1464.01 ^{ED}	88.7		
$^3F_2 + ^3F_3$	3H_4	4923.7	20.48 ^{ED} + 0.39 ^{MD}	0.4	4898.36	0.204
	3H_5	1581.3	590.23 ^{ED}	12.0		
	3F_4	1118.1	818.81 ^{ED} + 72.33 ^{MD}	18.2		
	3H_6	684.2	3396.12 ^{ED}	69.4		
1G_4	$^3F_2 + ^3F_3$	1529.3	86.00 ^{ED} + 4.64 ^{MD}	3.1	2867.78	0.349
	3H_4	1166.9	257.70 ^{ED} + 39.56 ^{MD}	10.4		
	3H_5	777.4	845.70 ^{ED} + 161.92 ^{MD}	35.1		
	3F_4	645.9	215.47 ^{ED} + 13.49 ^{MD}	8.0		
	3H_6	472.7	1243.3 ^{ED}	43.4		
1D_2	1G_4	1519.1	188.17 ^{ED}	3.7	34688.5	0.029
	$^3F_2 + ^3F_3$	762.1	2320.43 ^{ED} + 185.66 ^{MD}	4.0		
	3H_4	659.9	2010.27 ^{ED}	5.8		
	3H_5	514.2	135.03 ^{ED}	0.4		
	3F_4	453.2	18445.5	53.2		
	3H_6	360.5	11403.4	32.9		

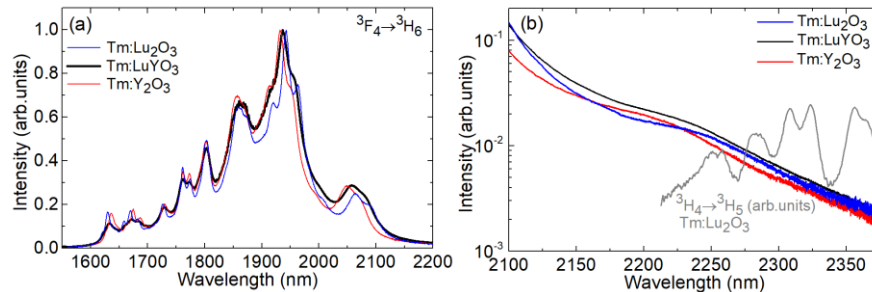
211 ^a $\langle\lambda_{\text{em}}\rangle$ - mean emission wavelength, $A_{\Sigma}^{\text{calc}}(JJ')$ - probability of spontaneous transitions, $B(JJ')$ -
 212 luminescence branching ratio, A_{tot} - total probability of spontaneous transitions from an excited-
 213 state, τ_{rad} - radiative lifetime.

214 3.3 Emission (spectra and lifetimes)

215 The Tm^{3+} luminescence was excited at ~ 796 nm using a CW Ti:Sapphire laser and the spectra
 216 were measured using an optical spectrum analyzer (OSA, AQ6376, Yokogawa) and a ZrF₄
 217 fiber. The spectral sensitivity of the set-up was calibrated using a 20 W quartz iodine lamp.

218 The normalized RT emission spectra of Tm^{3+} ions in the LuYO_3 , Y_2O_3 and Lu_2O_3
 219 ceramics are shown in Fig. 6(a). The observed emission is related to the ${}^3\text{F}_4 \rightarrow {}^3\text{H}_6$ transition.
 220 The spectra are very broad spanning from 1.6 up to 2.35 μm . For the “mixed” ceramic, the
 221 spectrum exhibits a notable inhomogeneous broadening as compared to those of the parent
 222 compounds. The spectral maximum is found at ~ 1936 nm. For the quasi-three-level
 223 ${}^3\text{F}_4 \rightarrow {}^3\text{H}_6$ Tm^{3+} laser, emission is expected at the long-wave wing of the luminescence
 224 spectrum. For Tm^{3+} -doped cubic sesquioxides, a broad peak above 2 μm is observed where
 225 maximum laser gain will occur. For the $\text{Tm}:\text{LuYO}_3$ ceramic, it is centered at 2058 nm, in
 226 between the positions for $\text{Tm}:\text{Y}_2\text{O}_3$ (2049 nm) and $\text{Tm}:\text{Lu}_2\text{O}_3$ (2063 nm). The emission
 227 bandwidth for this peak also exceeds those for the parent compounds supporting our
 228 assumption about the formation of a solid-solution.

229 A careful examination of the long-wave part of the luminescence spectra of all the studied
 230 ceramics indicates that their emission extends up to at least 2.35 μm (further measurement
 231 was limited by the sensitivity of our set-up). It is associated with the ${}^3\text{F}_4 \rightarrow {}^3\text{H}_6$ transition of
 232 Tm^{3+} according to the luminescence decay studies: the luminescence lifetime remains nearly
 233 constant when changing the detection wavelength between 1.8 – 2.3 μm . One may argue that
 234 such long-wave emission may also partially originate from the ${}^3\text{H}_4 \rightarrow {}^3\text{H}_5$ electronic transition
 235 [40]. However, no characteristic spectral features of this transition are found in the spectra.
 236 To prove this, we have used a low-doped (<0.1 at.%) $\text{Tm}:\text{Lu}_2\text{O}_3$ crystal exhibiting almost no
 237 self-quenching of the ${}^3\text{H}_4$ lifetime to measure the luminescence spectrum of the ${}^3\text{H}_4 \rightarrow {}^3\text{H}_5$
 238 transition, Fig. 6(b). It reveals several well-resolved emission peaks centered at 2282, 2308,
 239 2324 and 2356 nm which are not found in the spectra of the ceramics. In contrast, the long-
 240 wave part of the emission spectrum of the ceramics is almost structureless and follows an
 241 exponential law at >2.25 μm , as seen from Fig. 6(b) plotted in a semi-log scale.



242

243 **Fig. 6.** (a,b) RT luminescence spectra of $\text{Tm}:\text{LuYO}_3$, $\text{Tm}:\text{Y}_2\text{O}_3$ and $\text{Tm}:\text{Lu}_2\text{O}_3$ ceramics
 244 around 2 μm : (a) overview of the spectra, (b) a close look at the 2100 – 2375 nm range, semi-
 245 log scale, grey curve – emission spectrum for the ${}^3\text{H}_4 \rightarrow {}^3\text{H}_5$ Tm^{3+} transition in a low-doped
 246 (<0.1 at.%) $\text{Tm}:\text{Lu}_2\text{O}_3$ shown for comparison. $\lambda_{\text{exc}} = 796$ nm.

247 The long-wave limit for purely electronic transitions ${}^3\text{F}_4 \rightarrow {}^3\text{H}_6$ is determined by the
 248 crystal-field splitting of the involved multiplets and, in particular, by the energy gap between
 249 the lowest sub-level of the ${}^3\text{F}_4$ state (5643 cm^{-1} , Y_1) and the highest sub-level of the ${}^3\text{H}_6$
 250 ground-state (810 cm^{-1} , Z_{13} , see below) [41]. This yields a value of 2069 nm. All the
 251 emissions above this wavelength are multiphonon-assisted (or vibronic) as they are related to
 252 the coupling between electrons and host vibrations (phonons) [42].

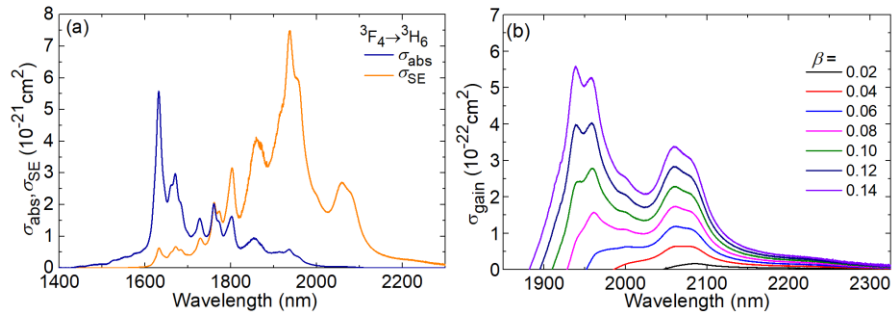
253 The very broad peak centered at 2.23 μm (for $\text{Tm}:\text{LuYO}_3$) is interpreted as a phonon
 254 sideband, see [42,43] for this term. Note that it takes an intermediate position between those
 255 for $\text{Tm}:\text{Y}_2\text{O}_3$ (2.21 μm) and $\text{Tm}:\text{Lu}_2\text{O}_3$ (2.25 μm) which agrees with the difference in the
 256 crystal-field strengths. This indicates that the position of this peak could be linked to those of
 257 electronic transitions. Indeed, for the “mixed” ceramic, the energy gap between the prominent

258 electronic emission band centered at 2058 nm and the above-described sideband (2236 nm) is
 259 $\sim 387 \text{ cm}^{-1}$. This well matches the most intense Raman peak of this material corresponding to
 260 vibration with an energy $h\nu_{\text{ph}} = 385.4 \text{ cm}^{-1}$, Fig. 3(b). Thus, one can describe the appearance
 261 of the phonon sideband in the Tm^{3+} emission spectrum as transitions to a virtual energy level
 262 located slightly above the highest electronic sub-levels of the ${}^3\text{H}_6$ multiplet [44], i.e., having
 263 an energy $E(Z_{13}) + h\nu_{\text{ph}}$.

264 The stimulated-emission (SE) cross-sections, σ_{SE} , for the ${}^3\text{F}_4 \rightarrow {}^3\text{H}_6$ transition of Tm^{3+}
 265 ions in the LuYO_3 ceramic were calculated using two methods, namely, (i) the reciprocity
 266 method [45], and (ii) the Füchtbauer – Ladenburg (F-L) formula [46]. The σ_{SE} spectra
 267 obtained by both methods were in good agreement with each other, considering the effect of
 268 reabsorption on the measured emission spectrum. In the F-L formula, we have used a
 269 radiative lifetime of the ${}^3\text{F}_4$ state $\tau_{\text{rad}} = 3.85 \pm 0.1 \text{ ms}$ to fit the two methods which reasonably
 270 agrees with that determined using the J - O theory (4.18 ms). In Fig. 7(a), the combined SE
 271 cross-section spectrum is shown. The maximum σ_{SE} is $0.75 \times 10^{-20} \text{ cm}^2$ at 1937 nm and at
 272 longer wavelengths where the laser operation is expected, $\sigma_{\text{SE}} = 0.27 \times 10^{-20} \text{ cm}^2$ at 2059 nm.

273 The ${}^3\text{F}_4 \rightarrow {}^3\text{H}_6$ transition of Tm^{3+} ions represents a quasi-three-level laser scheme with
 274 reabsorption at the laser wavelength. Thus, the gain cross-sections, $\sigma_{\text{gain}} = \beta\sigma_{\text{SE}} - (1 - \beta)\sigma_{\text{abs}}$,
 275 are calculated, where $\beta = N_2({}^3\text{F}_4)/N_{\text{Tm}}$ is the population inversion ratio. The gain profiles of
 276 the “mixed” ceramic are shown in Fig. 7(b). The spectra are smooth and broad extending until
 277 $2.35 \mu\text{m}$. For small inversion ratios ($\beta < 0.10$), two local maxima appear in the spectra,
 278 centered at ~ 2085 and 2059 nm . For $\beta = 0.04$, the gain bandwidth (FWHM) is as broad as
 279 75 nm . For higher $\beta > 0.10$, the gain maxima experience a blue-shift to ~ 1960 and 1938 nm .
 280 The observed broadband gain properties indicate the high suitability of this ceramic for
 281 generation of sub-100 fs pulses.

282 The existence of gain at long wavelengths well above $2.1 \mu\text{m}$ due to the multiphonon-
 283 assisted transitions is an important prerequisite for generation of ultrashort pulses from mode-
 284 locked Tm sesquioxide lasers. Indeed, the emission spectra of such lasers delivering pulses in
 285 the sub-100 fs time domain contained spectral components extending up to $2.3 \mu\text{m}$ [30,47].

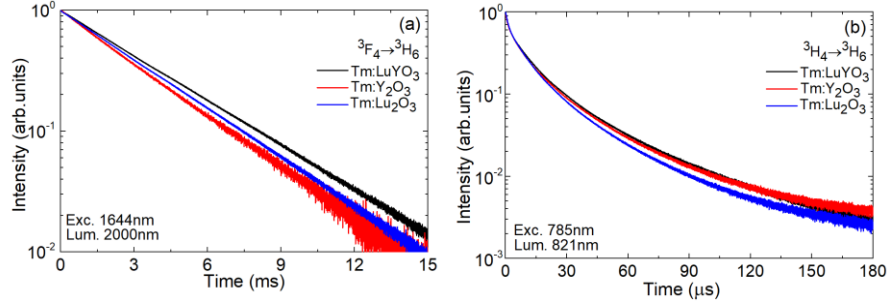


286
 287 **Fig. 7.** The ${}^3\text{H}_6 \leftrightarrow {}^3\text{F}_4$ transition of Tm^{3+} ions in the LuYO_3 ceramic: (a) absorption, σ_{abs} , and
 288 stimulated-emission (SE), σ_{SE} , cross-sections; (b) the gain cross-sections, $\sigma_{\text{gain}} = \beta\sigma_{\text{SE}} - (1 -$
 289 $\beta)\sigma_{\text{abs}}$, for different inversion ratios $\beta = N_2({}^3\text{F}_4)/N_{\text{Tm}}$.

290 The luminescence dynamics was studied using a ns optical parametric oscillator (Horizon,
 291 Continuum), a 1/4 m monochromator (Oriel 77200), an InGaAs detector and an 8 GHz digital
 292 oscilloscope (DSA70804B, Tektronix). To avoid the effect of reabsorption (radiation
 293 trapping) on the measured lifetimes, finely powdered samples were used.

294 For the ${}^3\text{F}_4$ Tm^{3+} state, the decay curves are well described by a single-exponential law,
 295 Fig. 8(a), yielding $\tau_{\text{lum}} = 3.470 \text{ ms}$ for the $\text{Tm}:\text{LuYO}_3$ ceramic. This value is slightly longer
 296 compared to the parent compounds, 3.224 ms ($\text{Tm}:\text{Lu}_2\text{O}_3$) and 2.919 ms ($\text{Tm}:\text{Y}_2\text{O}_3$). Note
 297 that the measured luminescence lifetimes of the ${}^3\text{F}_4$ state for the studied sesquioxide ceramics
 298 are close to those obtained for single-crystals with low Tm^{3+} doping levels ($< 0.3 \text{ at.}\%$), i.e.,

299 3.38 ms (Tm:Lu₂O₃) and 3.54 ms (Tm:Y₂O₃) [7], indicating a relatively weak concentration
 300 quenching.



301

302

303

304

Fig. 8. RT luminescence decay curves for Tm³⁺ ions in the LuYO₃, Y₂O₃, and Lu₂O₃ ceramics:
 (a) decay from the ³F₄ state, λ_{exc} = 1644 nm, λ_{lum} = 2000 nm; (b) decay from the ³H₄ state,
 λ_{exc} = 785 nm, λ_{lum} = 821 nm. Powdered samples.

305

306

307

308

309

310

311

312

313

For the ³H₄ pump level, the decay is clearly not single-exponential, Fig. 8(b), owing to the
 efficient cross-relaxation (CR) process, ³H₄ + ³H₆ → ³F₄ + ³F₄. For the Tm:LuYO₃ ceramics,
 the mean luminescence lifetime of the ³H₄ state <τ_{lum}> is only 24 μs. It is much shorter than
 the so-called intrinsic lifetime (measured at a very low Tm³⁺ doping level, i.e., unaffected by
 the CR process), τ_{lum,0} = 350 μs for Tm:Lu₂O₃ [7]. Thus, the estimated CR rate,
 W_{CR} = (1/τ_{lum}) - (1/τ_{lum,0}), is about 3.88 × 10⁴ s⁻¹ (for 3 at.% Tm³⁺ doping). The CR rate is
 quadratically proportional to the doping concentration, W_{CR} = C_{CR}(N_{Tm})² [48], where
 C_{CR} = 0.56 × 10⁻³⁷ cm⁶s⁻¹ is the concentration-independent CR parameter.

Table 3 summarizes the measured luminescence lifetimes.

314

315

**Table 3. Measured Luminescence Lifetimes of the ³F₄ and ³H₄ Tm³⁺ States in the
 LuYO₃, Y₂O₃ and Lu₂O₃ Ceramics.**

Ceramic	τ _{lum} , ms	
	³ H ₄	³ F ₄
LuYO ₃	0.024	3.470
Y ₂ O ₃	0.025	2.919
Lu ₂ O ₃	0.022	3.224

316

3.4 Low-temperature spectroscopy

317

318

319

For low temperature (LT, 12 K) studies, the samples were mounted in an APD DE-202
 closed-cycle cryo-cooler equipped with an APD HC 2 Helium vacuum cryo-compressor and a
 Laceshore 330 temperature controller.

320

321

322

323

324

325

326

327

328

329

330

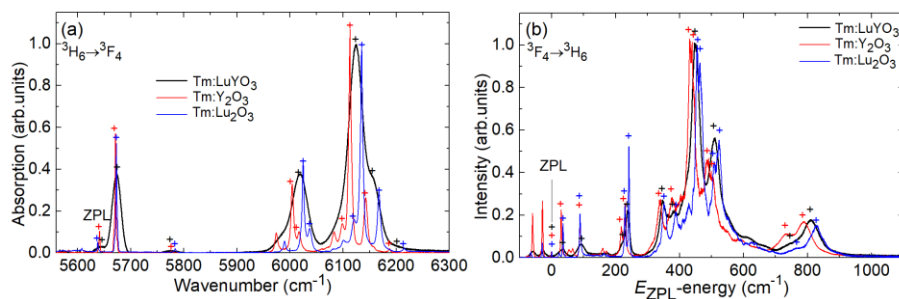
331

332

333

334

The ³H₆ → ³F₄ (absorption) and ³F₄ → ³H₆ (luminescence) Tm³⁺ transitions were
 considered giving access to the crystal-field splitting of both multiplets. In Fig. 9, the
 obtained LT absorption spectra are plotted vs. the photon energy and the LT emission
 spectra – vs. (E_{ZPL} – photon energy). The considered transitions are of pure ED nature and
 thus no signatures of C_{3i} sites could be observed. For the RE³⁺ ions in C₂ sites, each multiplet
^{2S+1}L_J with an integer J is split into a total of 2J + 1 sub-levels. A careful examination of the
 LT spectra of the parent compounds allowed us to determine the full set of Stark sub-levels
 for both multiplets, cf. Table 4. Here, we use the empirical notations for the electronic levels
 proposed by Lupei *et al.* [49]: ³H₆ = Z_i (i = 1...13) and ³F₄ = Y_j (j = 1...9). The total Stark
 splitting of the ground-state, ΔE(³H₆), increased in the R = Y → Lu series, from 788 to
 828 cm⁻¹. The peaks corresponding to electronic transitions were relatively narrow and
 experienced a notable shift between Y₂O₃ and Lu₂O₃ according to the different crystal-field
 strengths in these compounds. For the most intense electronic line in absorption, designated
 as Z₀ → Y₇, the peak positions / widths are 6112.8 / 6.1 cm⁻¹ (Y₂O₃) and 6134.9 / 5.5 cm⁻¹
 (Lu₂O₃), respectively.



335

336

337

338

Fig. 9. Low-temperature (LT, 12 K) spectroscopy of Tm^{3+} ions in the LuYO_3 , Y_2O_3 , Lu_2O_3 ceramics: (a) absorption spectra, the ${}^3\text{H}_6 \rightarrow {}^3\text{F}_4$ transition; (b) luminescence spectra, the ${}^3\text{F}_4 \rightarrow {}^3\text{H}_6$ transition, ZPL – zero-phonon-lines, “+” indicate the assigned electronic transitions.

339

340

341

342

343

344

345

346

347

348

349

350

351

For the “mixed” ceramic, the LT spectroscopy does not reveal any signatures of two distinct Tm^{3+} species (e.g., the presence of two sets of electronic transitions or any dependence of the luminescence spectrum on the excitation wavelength). Instead, the electronic lines in both the LT absorption and emission spectra are notably broadened and their peak positions take an intermediate place between those for the parent compounds. E.g., the above-mentioned $Z_0 \rightarrow Y_7$ Tm^{3+} absorption line shifts to 6123.9 cm^{-1} and its width increases to 34.8 cm^{-1} (~5 times that of $\text{Tm:Lu}_2\text{O}_3$). This confirms the formation of a substitutional solid-solution $(\text{Lu}_{1-x}\text{Y}_x)_2\text{O}_3$ with a mixture of the host-forming cations at the atomic level. The compositional disorder originates from the second coordination sphere of Tm^{3+} ions formed by different sets of Lu^{3+} and Y^{3+} cations with different ionic radii. Thus, strictly speaking, one cannot speak about a predominant substitution of the host-forming Y^{3+} or Lu^{3+} cations by the dopant Tm^{3+} ones. Table 3 presents an attempt to assign the Stark sub-levels of the Tm^{3+} ion in the LuYO_3 ceramic.

352

353

Table 4. Experimental Crystal-Field Splitting of the ${}^3\text{H}_6$ and ${}^3\text{F}_4$ Tm^{3+} Multiplets in LuYO_3 , Y_2O_3 , and Lu_2O_3 Ceramics

$E({}^3\text{H}_6), \text{cm}^{-1}$				$E({}^3\text{F}_4), \text{cm}^{-1}$			
Z_i	Y_2O_3	Lu_2O_3	LuYO_3	Y_j	Y_2O_3	Lu_2O_3	LuYO_3
Z_1	0	0	0	Y_1	5612	5608	5643
Z_2	30	35	36	Y_2	5671	5673	5674
Z_3	89	88	94	Y_3	5776	5784	5773
Z_4	217	229	221	Y_4	6004	6024	6019
Z_5	229	241	239	Y_5	6016	6037	
Z_6	338	352	347	Y_6	6099	6120	6124
Z_7	376	388	383	Y_7	6113	6134	
Z_8	432	455	449	Y_8	6142	6167	6156
Z_9	439	463		Y_9	6187	6215	6203
Z_{10}	486	508	509				
Z_{11}	503	523					
Z_{12}	732	764	747				
Z_{13}	788	828	810				

354

355

356

357

358

359

360

361

362

A similar analysis for Yb^{3+} ions in a mixed $(\text{Lu,Sc})_2\text{O}_3$ sesquioxide crystal was performed recently in [50,51] however not going down to temperatures of about 10 K. The authors have shown a tendency for increasing the crystal-field strengths in R_2O_3 sesquioxides with decreasing the R^{3+} ionic radius (which agrees with our analysis, as $R(\text{Y}^{3+}) = 0.90 \text{ \AA}$ and $R(\text{Lu}^{3+}) = 0.861 \text{ \AA}$ for a VI-fold oxygen coordination). They also observed a monotonous shift of the energies of Yb^{3+} Stark sub-levels with the Lu/Sc ratio. One can expect a monotonous variation of the barycenter multiplet energies of Tm^{3+} ions in $(\text{Lu}_{1-x}\text{Y}_x)_2\text{O}_3$ solid-solutions with changing the Lu/Y ratio.

363

4. Conclusion

364 In the present work, we tried to reveal the effect of a “mixed” host composition on the
365 spectroscopic properties of the dopant Tm^{3+} ions using the cubic sesquioxide system (R_2O_3)
366 and analyzing a lutetia – yttria (LuYO_3) transparent ceramic fabricated by HIPing. Our study
367 evidences the formation of a substitutional sesquioxide solid-solution with a mixture of cations
368 at the atomic level according to the following findings: (i) the dominant peak in the Raman
369 spectrum characteristic to C-type bixbyite structure takes an intermediate position between
370 those for the parent compounds and is notably broadened; (ii) the absorption and emission
371 spectra of the Tm^{3+} ion exhibit significant inhomogeneous broadening; (iii) at 12 K, the
372 absorption / emission peaks corresponding to electronic transitions are notably broadened, their
373 positions follow the variation of the crystal-field strength in the $\text{R} = \text{Y} \rightarrow \text{Lu}$ series while no
374 evidence of two distinct Tm^{3+} species in C_2 sites with a second coordination sphere
375 predominantly formed by Lu^{3+} or Y^{3+} is observed.

376 The $\text{Tm}:\text{LuYO}_3$ ceramic benefits from inhomogeneously broadened emission related to
377 the ${}^3\text{F}_4 \rightarrow {}^3\text{H}_6$ transition naturally extending above $2\ \mu\text{m}$ (the limit set by the total Stark
378 splitting of the Tm^{3+} ground-state, $\Delta({}^3\text{H}_6) = 810\ \text{cm}^{-1}$). In addition, it exhibits a long-wave
379 emission observed up to at least $2.35\ \mu\text{m}$. The analysis of its spectral shape reveals a phonon
380 sideband at $2.23\ \mu\text{m}$ and a part with a nearly exponential dependence at longer wavelengths.
381 The phonon sideband is associated to the coupling of electronic transitions with the most
382 intense Raman mode of the C-type bixbyite structure (centered at $385.4\ \text{cm}^{-1}$ for LuYO_3) and
383 the exponential part – with multiphonon-assisted (vibronic) processes. All this leads to
384 smooth (structureless) and broad gain spectra of Tm^{3+} ions supporting the generation of
385 ultrashort (sub-100 fs) pulses. The utilization of multiphonon-assisted emission sidebands of
386 Tm^{3+} ions in sesquioxides may be a viable way for further pulse shortening in mode-locked
387 lasers emitting above $2\ \mu\text{m}$.

388 **Funding.** French Agence Nationale de la Recherche (ANR) SPLENDID2 (ANR-19-CE08-0028). “RELANCE”
389 Chair of Excellence project funded by the Normandy Region. The research at IChHPS RAS was funded by the
390 Russian Science Foundation (21-13-00397). National Natural Science Foundation of China (61975208, 61875199,
391 61905247, 52032009, 61850410533, 62075090, U21A20508); Sino-German Scientist Cooperation and Exchanges
392 Mobility Program (M-0040).

393 **Acknowledgment.** Xavier Mateos acknowledges the Serra Hünter program.

394 **Disclosures.** The authors declare no conflicts of interest.

395 **Data availability.** Data underlying the results presented in this paper are not publicly available at this time but
396 may be obtained from the authors upon reasonable request.

397 References

- 398 1. C. Kränkel, “Rare-earth-doped sesquioxides for diode-pumped high-power lasers in the 1-, 2-, and 3- μm
399 spectral range,” *IEEE J. Sel. Top. Quantum Electron.* **21**(1), 1602013–1–13 (2015).
- 400 2. Z. Liu, A. Ikesue, and J. Li, “Research progress and prospects of rare-earth doped sesquioxide laser
401 ceramics,” *J. Eur. Ceram. Soc.* **41**(7), 3895–3910 (2021).
- 402 3. P. A. Loiko, K. V. Yumashev, R. Schödel, M. Peltz, C. Liebald, X. Mateos, B. Deppe, and C. Kränkel,
403 “Thermo-optic properties of $\text{Yb}:\text{Lu}_2\text{O}_3$ single crystals,” *Appl. Phys. B* **120**(4), 601–607 (2015).
- 404 4. L. Laversenne, Y. Guyot, C. Goutaudier, M. T. Cohen-Adad, and G. Boulon, “Optimization of spectroscopic
405 properties of Yb^{3+} -doped refractory sesquioxides: cubic Y_2O_3 , Lu_2O_3 and monoclinic Gd_2O_3 ,” *Opt.*
406 *Mater.* **16**(4), 475–483 (2001).
- 407 5. R. P. Leavitt, J. B. Gruber, N. C. Chang, and C. A. Morrison, “Optical spectra, energy levels, and crystal-field
408 analysis of tripositive rare-earth ions in Y_2O_3 . II. Non-Kramers ions in C_2 sites,” *J. Chem. Phys.* **76**(10), 4775–
409 4788 (1982).
- 410 6. J. B. Gruber, R. P. Leavitt, C. A. Morrison, and N. C. Chang, “Optical spectra, energy levels, and crystal-field
411 analysis of tripositive rare-earth ions in Y_2O_3 . IV. C_{3i} sites,” *J. Chem. Phys.* **82**(12), 5373–5378 (1985).
- 412 7. P. Loiko, P. Koopmann, X. Mateos, J. M. Serres, V. Jambunathan, A. Lucianetti, T. Mocek, M. Aguiló, F. Díaz,
413 U. Griebner, V. Petrov, and C. Kränkel, “Highly-efficient, compact $\text{Tm}^{3+}:\text{RE}_2\text{O}_3$ ($\text{RE} = \text{Y}, \text{Lu}, \text{Sc}$) sesquioxide
414 lasers based on thermal guiding,” *IEEE J. Sel. Top. Quantum Electron.* **24**(5), 1600713–1–13 (2018).
- 415 8. L. Fornasiero, E. Mix, V. Peters, K. Petermann, and G. Huber, “Czochralski growth and laser parameters of
416 RE^{3+} -doped Y_2O_3 and Sc_2O_3 ,” *Ceram. Int.* **26**(6), 589–592 (2000).
- 417 9. C. Goutaudier, F. S. Ermeneux, M. T. Cohen-Adad, and R. Moncorge, “Growth of pure and RE^{3+} -doped Y_2O_3
418 single crystals by LHPG technique,” *J. Cryst. Growth* **210**(4), 693–698 (2000).

- 419
420
421
422
423
424
425
426
427
428
429
430
431
432
433
434
435
436
437
438
439
440
441
442
443
444
445
446
447
448
449
450
451
452
453
454
455
456
457
458
459
460
461
462
463
464
465
466
467
468
469
470
471
472
473
474
475
476
477
478
479
480
481
482
483
10. A. Ikesue and Y. L. Aung, "Ceramic laser materials," *Nat. Photon.* **2**(12), 721–727 (2008).
 11. J. Lu, K. Takaichi, T. Uematsu, A. Shirakawa, M. Musha, K. I. Ueda, H. Yagi, T. Yanagitani, and A. A. Kaminskii, "Yb³⁺:Y₂O₃ ceramics—a novel solid-state laser material," *Jpn. J. Appl. Phys.* **41**(12A), L1373–L1375 (2002).
 12. P. A. Ryabochkina, A. N. Chabushkin, Y. L. Kopylov, V. V. Balashov, and K. V. Lopukhin, "Two-micron lasing in diode-pumped ceramics," *Quantum Electron* **46**(7), 597–600 (2016).
 13. K. Takaichi, H. Yagi, A. Shirakawa, K. Ueda, S. Hosokawa, T. Yanagitani, and A. A. Kaminskii, "Lu₂O₃:Yb³⁺ ceramics—a novel gain material for high-power solid-state lasers," *Phys. Status Solidi A* **202**(1), R1–R3 (2005).
 14. O. L. Antipov, A. A. Novikov, N. G. Zakharov, and A. P. Zinov'ev, "Optical properties and efficient laser oscillation at 2066 nm of novel Tm:Lu₂O₃ ceramics," *Opt. Mater. Express* **2**(2), 183–189 (2012).
 15. J. Lu, J. F. Bisson, K. Takaichi, T. Uematsu, A. Shirakawa, M. Musha, K. Ueda, H. Yagi, T. Yanagitani, and A. A. Kaminskii, "Yb³⁺:Sc₂O₃ ceramic laser," *Appl. Phys. Lett.* **83**(6) 1101–1103 (2003).
 16. W. Jing, P. Loiko, J. Maria Serres, Y. Wang, E. Vilejshikova, M. Aguiló, F. Díaz, U. Griebner, H. Huang, V. Petrov, and X. Mateos, "Synthesis, spectroscopy, and efficient laser operation of "mixed" sesquioxide Tm:(Lu,Sc)₂O₃ transparent ceramics," *Opt. Mater. Express* **7**(11), 4192–4202 (2017).
 17. J. Saikawa, Y. Sato, T. Taira, and A. Ikesue, "Passive mode locking of a mixed garnet Yb:Y₃ScAl₄O₁₂ ceramic laser," *Appl. Phys. Lett.* **85**(24), 5845–5847 (2004).
 18. A. Pirri, B. Patrizi, R. N. Maksimov, V. A. Shitov, V. V. Osipov, M. Vannini, and G. Toci, "Spectroscopic investigation and laser behaviour of Yb-doped laser ceramics based on mixed crystalline structure (Sc_xY_{1-x})₂O₃," *Ceram. Int.* **47**(20), 29483–29489 (2021).
 19. A. Schmidt, V. Petrov, U. Griebner, R. Peters, K. Petermann, G. Huber, C. Fiebig, K. Paschke, and G. Erbert, "Diode-pumped mode-locked Yb:LuScO₃ single crystal laser with 74 fs pulse duration," *Opt. Lett.* **35**(4), 511–513 (2010).
 20. C. Kränkel, A. Uvarova, É. Haurat, L. Hülshoff, M. Brützam, C. Gugushev, S. Kalusniak, and D. Klimm, "Czochralski growth of mixed cubic sesquioxide crystals in the ternary system Lu₂O₃–Sc₂O₃–Y₂O₃," *Acta Crystallogr. B. Struct. Sci. Cryst. Eng. Mater.* **77**(4), 550–558 (2021).
 21. W. Jing, P. Loiko, J. M. Serres, Y. Wang, E. Kifle, E. Vilejshikova, M. Aguiló, F. Díaz, U. Griebner, H. Huang, and V. Petrov, "Synthesis, spectroscopic characterization and laser operation of Ho³⁺ in "mixed" (Lu,Sc)₂O₃ ceramics," *J. Lumin.* **203**, 145–151 (2018).
 22. L. Basyrova, P. Loiko, W. Jing, Y. Wang, H. Huang, E. Dunina, A. Kornienko, L. Fomicheva, B. Viana, U. Griebner, V. Petrov, M. Aguiló, F. Díaz, X. Mateos, and P. Camy, "Spectroscopy and efficient laser operation around 2.8 μm of Er:(Lu,Sc)₂O₃ sesquioxide ceramics," *J. Lumin.* **240**, 118373–1–11 (2021).
 23. X. Xu, Z. Hu, D. Li, P. Liu, J. Zhang, B. Xu, and J. Xu, "First laser oscillation of diode-pumped Tm³⁺-doped LuScO₃ mixed sesquioxide ceramic," *Opt. Express* **25**(13), 15322–15329 (2017).
 24. Z. Hao, L. Zhang, Y. Wang, H. Wu, GH. Pan, H. Wu, X. Zhang, D. Zhao, and J. Zhang, "11 W continuous-wave laser operation at 2.09 μm in Tm:Lu_{1.6}Sc_{0.4}O₃ mixed sesquioxide ceramics pumped by a 796 nm laser diode," *Opt. Mater. Express* **8**(11), 3615–3621 (2018).
 25. W. Jing, P. Loiko, L. Basyrova, Y. Wang, H. Huang, P. Camy, U. Griebner, V. Petrov, J. M. Serres, R. M. Solé, M. Aguiló, F. Díaz, and X. Mateos, "Spectroscopy and laser operation of highly-doped 10 at.% Yb:(Lu,Sc)₂O₃ ceramics," *Opt. Mater.* **117**, 111128–1–7 (2021).
 26. P. Koopmann, S. Lamrini, K. Scholle, P. Fuhrberg, K. Petermann, and G. Huber, "Efficient diode-pumped laser operation of Tm:Lu₂O₃ around 2 μm," *Opt. Lett.* **36**(6), 948–950 (2011).
 27. A. Suzuki, C. Kränkel, and M. Tokurakawa, "High quality-factor Kerr-lens mode-locked Tm:Sc₂O₃ single crystal laser with anomalous spectral broadening," *Appl. Phys. Express* **13**(5), 052007–1–4 (2020).
 28. Y. Wang, W. Jing, P. Loiko, Y. Zhao, H. Huang, X. Mateos, S. Suomalainen, A. Härkönen, M. Guina, U. Griebner, and V. Petrov, "Sub-10 optical-cycle passively mode-locked Tm:(Lu_{2/3}Sc_{1/3})₂O₃ ceramic laser at 2 μm," *Opt. Express* **26**(8), 10299–10304 (2018).
 29. Y. Zhao, L. Wang, W. Chen, Z. Pan, Y. Wang, P. Liu, X. Xu, Y. Liu, D. Shen, J. Zhang, M. Guina, X. Mateos, P. Loiko, Z. Wang, X. Xu, J. Xu, M. Mero, U. Griebner, and V. Petrov, "SESAM mode-locked Tm:LuYO₃ ceramic laser generating 54-fs pulses at 2048 nm," *Appl. Opt.* **59**(33), 10493–10497 (2020).
 30. Y. Zhao, L. Wang, Y. Wang, J. Zhang, P. Liu, X. Xu, Y. Liu, D. Shen, J. E. Bae, T. G. Park, F. Rotermund, X. Mateos, P. Loiko, Z. Wang, X. Xu, J. Xu, M. Mero, U. Griebner, V. Petrov, and W. Chen, "SWCNT-SA mode-locked Tm:LuYO₃ ceramic laser delivering 8-optical-cycle pulses at 2.05 μm," *Opt. Lett.* **45**(2), 459–462 (2020).
 31. Y. Repelin, C. Proust, E. Husson, and J. M. Beny, "Vibrational spectroscopy of the C-form of yttrium sesquioxide," *J. Solid State Chem.* **118**(1), 163–169 (1995).
 32. N. D. Todorov, M. V. Abrashev, V. Marinova, M. Kadiyski, L. Dimowa, and E. Faulques, "Raman spectroscopy and lattice dynamical calculations of Sc₂O₃ single crystals," *Phys. Rev. B* **87**(10), 104301–1–5 (2013).
 33. D. E. Zelmon, J. M. Northridge, N. D. Haynes, D. Perlov, and K. Petermann, "Temperature-dependent Sellmeier equations for rare-earth sesquioxides," *Appl. Opt.* **52**(16), 3824–3828 (2013).
 34. D. Zhang, W. Lin, Z. Lin, L. Jia, W. Zheng, and F. Huang, "Lu₂O₃: A promising ultrawide bandgap semiconductor for deep UV photodetector," *Appl. Phys. Lett.* **118**(21), 211906–1–4 (2021).
 35. B. R. Judd, "Optical absorption intensities of rare-earth ions," *Phys. Rev.* **127**(3), 750–761 (1962).
 36. G. S. Ofelt, "Intensities of crystal spectra of rare-earth ions," *J. Chem. Phys.* **37**(3), 511–520 (1962).

- 484
485
486
487
488
489
490
491
492
493
494
495
496
497
498
499
500
501
502
503
504
505
506
507
508
509
510
511
512
513
514
515
516
517
518
519
520
37. A. A. Kornienko and E. B. Dunina, "Determination of intensity parameters from the fine details of the Stark structure in the energy spectrum of Tm^{3+} ions in $\text{Y}_3\text{Al}_5\text{O}_{12}$," *Opt. Spectrosc.* **97**(1), 68–75 (2004).
 38. L. Zhang, H. Lin, G. Zhang, X. Mateos, J. Maria Serres, M. Aguiló, F. Díaz, U. Griebner, V. Petrov, Y. Wang, P. Loiko, E. Vileshnikova, K. Yumashev, Z. Lin, and W. Chen, "Crystal growth, optical spectroscopy and laser action of Tm^{3+} -doped monoclinic magnesium tungstate," *Opt. Express* **25**(4), 3682–3693 (2017).
 39. R. Moncorgé, Y. Guyot, C. Kränkel, K. Lebbou, and A. Yoshikawa, "Mid-infrared emission properties of the Tm^{3+} -doped sesquioxide crystals Y_2O_3 , Lu_2O_3 , Sc_2O_3 and mixed compounds $(\text{Y,Lu,Sc})_2\text{O}_3$ around 1.5-, 2- and 2.3- μm ," *J. Lumin.* **241**, 118537-1–9 (2022).
 40. L. Guillemot, P. Loiko, R. Soulard, A. Braud, J. L. Doualan, A. Hideur, and P. Camy, "Close look on cubic $\text{Tm}:\text{KY}_3\text{F}_{10}$ crystal for highly efficient lasing on the $^3\text{H}_4 \rightarrow ^3\text{H}_5$ transition," *Opt. Express* **28**(3), 3451–3463 (2020).
 41. P. Loiko, E. Kifle, L. Guillemot, J. L. Doualan, F. Starecki, A. Braud, M. Aguiló, F. Díaz, V. Petrov, X. Mateos, and P. Camy, "Highly efficient 2.3 μm thulium lasers based on a high-phonon-energy crystal: evidence of vibronic-assisted emissions," *J. Opt. Soc. Am. B* **38**(2), 482–495 (2021).
 42. S. Tanabe, K. Hirao, and N. Soga, "Local structure of rare-earth ions in fluorophosphate glasses by phonon sideband and Mössbauer spectroscopy," *J. Non-Cryst. Solids* **142**, 148–154 (1992).
 43. F. Auzel, "Multiphonon-assisted anti-Stokes and Stokes fluorescence of triply ionized rare-earth ions," *Phys. Rev. B* **13**(7), 2809–2817 (1976).
 44. P. Loiko, X. Mateos, S. Y. Choi, F. Rotermund, J. M. Serres, M. Aguiló, F. Díaz, K. Yumashev, U. Griebner, and V. Petrov, "Vibronic thulium laser at 2131 nm Q-switched by single-walled carbon nanotubes," *J. Opt. Soc. Am. B* **33**(11), D19–D27 (2016).
 45. S. A. Payne, L. L. Chase, L. K. Smith, W. L. Kway, and W. F. Krupke, "Infrared cross-section measurements for crystals doped with Er^{3+} , Tm^{3+} and Ho^{3+} ," *IEEE J. Quantum Electron.* **28**(11), 2619–2630 (1992).
 46. B. F. Aull and H. P. Jenssen, "Vibronic interactions in Nd:YAG resulting in nonreciprocity of absorption and stimulated emission cross sections," *IEEE J. Quantum Electron.* **18**(5), 925–930 (1982).
 47. Y. Zhao, L. Wang, W. Chen, P. Loiko, Y. Wang, Z. Pan, H. Yang, W. Jing, H. Huang, J. Liu, X. Mateos, Z. Wang, X. Xu, U. Griebner, and V. Petrov, "Kerr-lens mode-locked Tm-doped sesquioxide ceramic laser," *Opt. Lett.* **46**(14), 3428–3431 (2021).
 48. P. Loiko, and M. Pollnau, "Stochastic model of energy-transfer processes among rare-earth ions. Example of $\text{Al}_2\text{O}_3:\text{Tm}^{3+}$," *J. Phys. Chem. C* **120**(46), 26480–26489 (2016).
 49. A. Lupei, V. Lupei, S. Grecu, C. Tiseanu, and G. Boulon, "Crystal-field levels of Tm^{3+} in gadolinium gallium garnet," *J. Appl. Phys.* **75**(9), 4652–4657 (1994).
 50. W. Liu, D. Lu, S. Pan, M. Xu, Y. Hang, H. Yu, H. Zhang, and J. Wang, "Ligand engineering for broadening infrared luminescence of Kramers ytterbium ions in disordered sesquioxides," *Cryst. Growth Des.* **19**(7), 3704–3713 (2019).
 51. R. Guo, D. Huang, D. Lu, F. Liang, Q. Zhang, H. Yu, and H. Zhang, "Spectral broadening mechanism of Yb^{3+} -doped cubic $\text{Lu}_x\text{Sc}_{2-x}\text{O}_3$ sesquioxide crystals for ultrafast lasers," *Opt. Mater. Express* **12**(5), 1963–1976 (2022).